ISSN 1330-3651 (Print), ISSN 1848-6339 (Online) https://doi.org/10.17559/TV-20220709090615
Original scientific papers

Multi-Response Optimization of Burnishing Variables for Minimizing Environmental Impacts

An-Le VAN, Trung-Thanh NGUYEN*

Abstract: The purpose of this investigation is to optimize minimum quantity lubrication (MQL) variables, including the nozzle diameter (*D*), inclined angle (*A*), air pressure (*P*), oil quantity (*F*), and spraying distance (*S*) for decreasing the energy consumption in the burnishing time (*EB*) and particulate matter index (*PI)* of the interior burnishing process. The optimal adaptive neuro-based-fuzzy inference system (ANFIS) models of the performance measures were proposed in terms of the MQL variables with the aid of the Taguchi method. The non-dominated sorting genetic algorithm based on the grid partitioning (NSGA-G) and TOPSI were employed to produce feasible solutions and determine the best optimal point. The obtained results indicated that the optimal values of the *D*, *A*, *P*, *F*, and *S* are 1.0 mm, 35 deg., 3 Bar, 70 ml/h, and 10 mm, respectively, while the *EB* and *PI* are decreased by 8.0% and 15.7% at the optimal solution. The optimal ANFIS models were trustworthy and ensure accurate predictions. The optimization technique comprising the ANFIS, NSGA-G, and TOPSIS could be extensively utilized to determine the optimal outcomes instead of the trial-error and/or human experience. The outcomes could help to decrease environmental impacts in the practical burnishing process.

Keywords: ANFIS; burnishing process; energy savings; genetic algorithm; particulate matter index

1 INTRODUCTION

Burnishing operation is considered as a prominent solution to produce the finishing surface and improve the mechanical properties (strength, wear rate, and corrosion resistance) of the burnished components. The burnishing process is widely applied to machining flat, external, and internal surfaces.

Conventionally, the surface characteristics (roughness indicators, hardness criteria, the depth of the hardened layer, geometrical deviations, wear rate, and coefficient of friction) of the burnished surface are primarily considered in former publications. The empirical models of the average roughness (*Ra*) and surface hardness (*SH*) of the burnished EN-9 steel were developed in terms of the burnishing force (*BF*), feed rate (*f*), roller contact width, and the number of passes (*N*) [1]. The authors stated that the *Ra* and *SH* could be decreased by 94.5% and 41.7%, respectively. The response surface method (RSM) was applied to develop predictive models of the *Ra*, *SH*, and the depth of the hardened layer in terms of the spindle speed (*S*), *f*, and burnishing depth (*BD*) for the AISI 1045 [2]. The results revealed that the optimal values of the *Ra*, *SH*, and the depth of the hardened layer were 0.10 μm, 38.1 HRC, and 93.5 μm, respectively. The impacts of the *BF*, *f*, and *N* on the *Ra* for burnished composite were analyzed by Cagan et al. [3]. The authors stated that the minimum *Ra* could be obtained at the *BF* of 250 N, the *f* of 0.05 mm/rev, the *N* of 4. The empirical models of the Ra, SH, and roundness were developed for the burnished Mg-SiC composite [4]. The outcomes presented that the optimum *Ra* of 0.1506 μm, the *SH* of 57.9996 HV, and the roundness of 0.0151 mm were obtained at the selected optimality. The cylindricity, circularity, dimensional deviation, and *Ra* of the burnished AISI 5150 were decreased by 80.8%, 2.1%, 48.0%, and 54.4%, respectively using optimal values of the *S*, *f*, and *BD*, in which the Taguchi and combined compromise solution methods were utilized [5]. The optimal data of MQL variables, including the nozzle diameter (*D*), inclined angle (*A*), lubricant quantity (*F*), and air pressure (*P*) were selected to decrease the cylindricity, circularity, and *Ra* of the internal burnishing process [6]. The authors stated that the cylindricity, circularity, and *Ra* could be decreased by 53.14%, 57.83%, and 72.97%, respectively. The artificial neural network (ANN) was applied to find optimal values of the *D*, *A*, *F*, and *P* for decreasing the maximum roughness and improving *SH* for the roller burnishing process [7]. The results indicated that the roughness and hardness were enhanced by 17.0% and 14.0%, respectively, as compared to common values. The process parameters of the MQL-based diamond burnishing operation, including the *S*, *f*, and *BF* were optimized using the RSM and desirability approach to decrease the *Ra* and *SH* [8]. The optimal data revealed that the *Ra* of 0.07 μm and *SH* of 363 HV were achieved using the optimal data. Similarly, Sachin et al. indicated that the *f* of 0.053 mm/rev, the *S* of 780 rpm, and *BF* of 200 N could be applied to yield a minimum Raand maximum SH in the cryogenic diamond burnishing operation [9]. Revankar et al. indicated that the specific wear rate and frictional coefficient of the burnished Ti-6Al-4V were decreased by 52.0% and 64.0%, respectively using the Taguchi method, as compared to the turned surface [10]. Attabi et al. emphasized that the *Ra* and wear loss of the burnished AISI 316L could be enhanced by 93.4% and 53.4%, respectively with the support of the ball burnishing operation [11].

With increasing energy prices and environmental legislation, minimizing negative impacts on the environment for different burnishing operations has been considered by many researchers. The optimal values of the *S*, *f*, and *BD* were selected to improve the power factor as well as energy consumption (*EB*) and decrease the *R*a for the flat burnishing operation [12]. The authors stated that improvements in the power factor, *EB*, and *Ra* were 22.0%, 49.5%, and 13.8%, respectively. The ANFIS approach was applied to present the correlations between process parameters (*S*, *f*, *BD*, and *N*) and the burnishing outputs (energy efficiency, machining noise, and *Ra*) [13]. The optimal values presented that the reductions in the energy efficiency, machining noise, and *Ra* were 6.98%, 25.0%, and 2.23%, respectively. The ANFIS and particle swarm optimization were utilized to find the optimum parameters of the ultrasonic-based burnishing process [14]. The results indicated that the *EB* and *Ra* were decreased by 33.0% and 16.0%, respectively. The *EB*, mean roughness, and roundness models of the MQL-assisted burnishing

operation were proposed in terms of the S, *f*, *F*, and *P* [15]. The authors stated that *EB*, mean roughness, and roundness deviation were decreased by 12.2%, 14.2%, and 42.5%, respectively at the optimality. The optimal values of the spraying distance (*S*), *A*, *P*, and *F* were selected to decrease the carbon emission, particulate matter index (*PI*), and the maximum roughness of the diamond burnishing process [16]. The author stated that the carbon emission, *PI*, and roughness were decreased by 3.8%, 26.5%, and 11.6%, respectively.

As a result, the performance measures, including the surface properties and environmental indicators of different burnishing processes have been enhanced, in which the process parameters and MQL variables are optimizing inputs. Moreover, various optimization approaches, such as the Taguchi method, ANN, ANFIS, RSM, and desirability approach were applied to find the optimal outcomes. However, the shortcomings of published works can be listed as follows:

The *EB* and *PI* models were developed for the flat and external burnishing operations. However, predictive models of the *EB* and *PI* regarding MQL variables for the internal burnishing process have not been proposed.

The impacts of MQL variables, including the *D*, *A*, *P*, *F*, and *S* on the *EB* and *PI* for the internal burnishing process have not been investigated. The proper selection of MQL variables significantly increases the cooling-lubrication (CL) effectiveness and air quality in the working space.

The selection of optimal MQL variables for decreasing the *EB* and *PI* values of the internal burnishing process has not been addressed. To boost the applicability of the burnishing process, finding optimal conditions for minimizing environmental impacts is an urgent demand.

In this investigation, the *EB* and *PI* values of the MQL-based interior burnishing operation are minimized using optimal MQL variables. The optimal ANFIS correlations are utilized to model performance measures, while the NSGA-G and TOPSIS are employed to generate optimality. The scientific remarks are expressed as:

The optimizing method having the ANFIS, NSGA-G, and TOPSIS can be utilized to deal with complicated optimization problems of other burnishing activities for determining global results. The optimal ANFIS architecture should be selected to describe highly nonlinear data. The optimal data of other manufacturing processes can be obtained using the developed method.

The observed data showing the influences of the MQL variables on the *EB* and *PI* objectives will support the operators realize the technological insights of the internal burnishing process.

The optimal outcomes are named as effective recommendations to propose sustainability-based burnishing operations and future works.

The Pareto graph presenting the relation between the *EB* and *PI* can be applied to find the optimum values of burnishing responses and MQL variables.

2 OPTIMIZATION APPROACH

The schematic of the internal burnishing operation with the MQL variables is shown in Fig. 1. The MQL variables and their values are shown in Tab. 1. The nozzle diameter is adjusted by means of different nozzles and the dimensions are confirmed with previous works. The pressure values are changed based on the configuration of the air chamber and gauge. The lubricant quantity is adjusted with the support of the flow control valve. The spraying distance is selected based on the referenced values according to published works. Consequently, the optimizing subject is expressed as:

- Finding $X = [D, A, P, F, \text{and } S]$.
- Minimizing *EB* and *PI*.
- Constraints: $0.5 \le D \le 1.5$ mm; $25 \le A \le 65$ deg.
- $2 \le P \le 6$ Bar; $30 \le F \le 80$ ml/h; $10 \le S \le 30$ mm.

Table 1 MQL system parameters for the experimental work

Symbol	Parameters	Values
D	Nozzle diameter / mm	0.5, 1.0, 1.5
A	Inclined angle / deg.	25, 45, 65
P	Air pressure / Bar	2, 4, 6
F	Lubricant quantity / ml/h	30, 50, 80
S	Spraying distance / mm	10, 20, 30

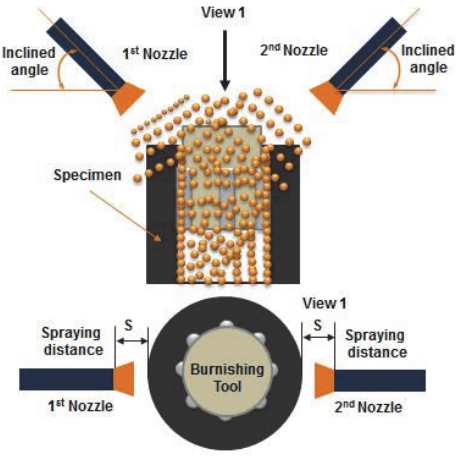

Figure 1 The schematic illustration of the internal burnishing operation

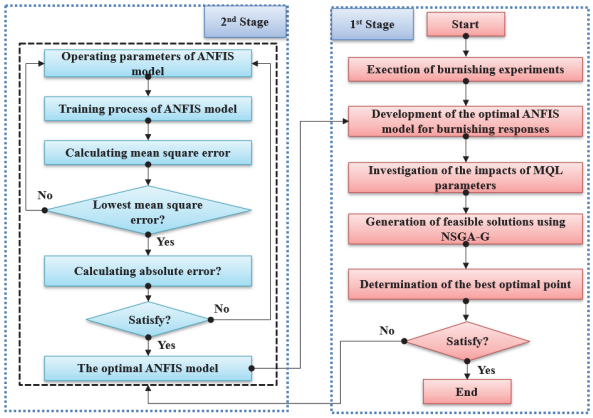

Figure 2 Optimization approach

The systematic approach for optimizing MQL variables is shown in Fig. 2.

Step 1: The physical experiments of the burnishing operation are conducted using the Box-Behnken design to save the experimental costs and trials.

The *EB* value is calculated as:

$$EB = P_m \times t_b \tag{1}$$

where P_m and t_b are machining power and burnishing time, respectively.

The *PI* value is calculated as:

$$PI = \frac{\sum_{i=1}^{n} PI_i}{n} \tag{2}$$

where PI_i presents the value of the particulate matter index 2.5 at the i-th time measured.

Step 2: The ANFIS models of the *EB* and *PI* are developed in terms of the MQL variables [17].

The Sugeno-based ANFIS model is applied to render the nonlinear relationships between inputs and responses.

Layer I: In the current layer, the inputs are converted to the fuzzy set using the membership functions. The outcomes of this layer are expressed as:

$$L_{1,i} = \mu_{Ai}(x), \qquad \text{for } i = 1, 2 \text{ or} \tag{3}$$

$$L_{1,i} = \mu_{Bi-2}(y), \qquad \text{for } i = 3, 4 \tag{4}$$

where x, y, A_i, and B_i denote the inputs and linguistic labels, respectively.

Layer II: In the current layer, the fixed nodes are generated, which are expressed as:

$$L_{2,i} = \omega_i = \mu_{Ai}(x) \times \mu_{Bi}(y) \tag{5}$$

where ω_i presents the firing strength.

Layer III: In the current layer, a normalized firing strength is expressed as:

$$L_{3,i} = \overline{\omega_i} = \frac{\omega_1}{\omega_1 + \omega_2}, \qquad \text{for } i = 1, 2. \tag{6}$$

Layer IV: In the current layer, consequent parameters are assigned to the normalized firing strength, which is expressed as:

$$L_{4,i} = \overline{\omega_i} f_i(x) = \overline{\omega_i}(p_i x + q_i x + r_i) \tag{7}$$

where p_i, q_i, and r_i are the consequent parameters, respectively.

Layer V: In the current layer, the summation of all incoming signals is computed:

$$L_{5,i} = \sum_i \overline{\omega_i} f_i = \frac{\sum_i \omega_i f_i}{\sum_i \omega_i} \tag{8}$$

The optimal architecture of each ANFIS model is selected using the mean square error (MSE), which is computed as:

$$MSE = \frac{1}{n} \sum_{i=1}^{n} (O_a - O_p)^2 \tag{9}$$

where O_a and O_p are the actual and predicted values, respectively.

Step 3: The optimal MQL variables and responses are selected using the NSGA-G algorithm. The operation steps of the NSGA-G are expressed as (Fig. 3):

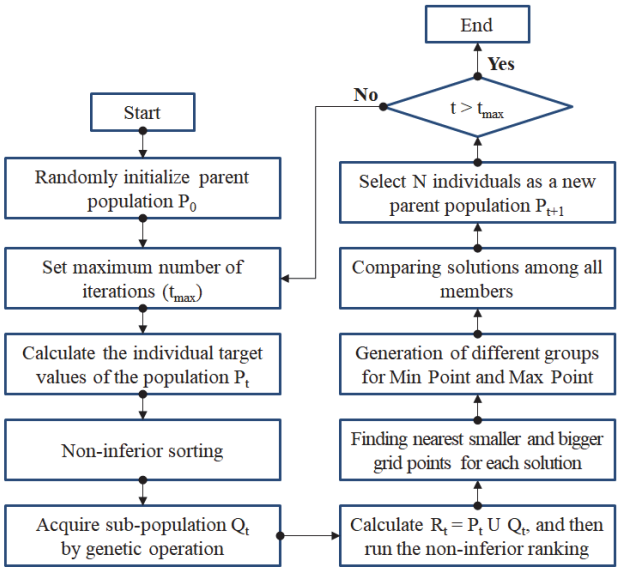

Figure 3 Operating principle of the NSGA-G

The parent population is executed based on the definition of the optimizing issue.

The parent population is divided into the number of the subsets (P_i), in which the subset P_{k+1} is dominated by the individual P_k. The individual P_i is expressed as:

$$P_i = \left\{ i / n_i, i \in \{1, 2, ..., N\} \right\} \tag{10}$$

The population P_k is expressed as:

$$P_k = \left\{ Allindividual / n_i - k + 1 \right\} \tag{11}$$

where n_i is the number of individuals in the population dominating.

The parent population with N size and offspring population with N members at t-th generation are produced with the aid of crossover and mutation operations.

The nearest smaller and bigger grid points of each solution were selected. The design space is divided into multi small groups.

The weak individuals are removed to form a new generation. The control loop is executed until the maximum number of generations is fit.

Step 4: The TOPSIS is utilized to select the best optimal point.

The normalized response is expressed as:

$$N_{ij} = \frac{o_{ij}}{\sqrt{\sum_{i=1}^{m} o_{ij}}} \tag{12}$$

where o_{ij} is the response value.

The positive point (P^+) and the negative point (N^-) are expressed as:

$$P_i^+ = \sqrt{\sum_{j=1}^{m} (o_{ij} - o_j^+)^2} \quad (13)$$

$$N_i^- = \sqrt{\sum_{j=1}^{m} (o_{ij} - o_j^-)^2} \quad (14)$$

The best solution is selected based on the highest score (*SC*), which is expressed as:

$$SC = \frac{N_i^-}{P_i^+ + N_i^-} \quad (15)$$

Table 2 Experimental data for the internal burnishing operation

No.	*D* / mm	*A* / deg.	*P* / Bar	*F* / ml/h	*S* / mm	*EB* / kJ	*PI* / mg/m³
1	1.0	65	4	55	10	52.88	131.8
2	1.0	45	2	30	20	56.03	109.5
3	1.0	25	4	80	20	51.29	137.9
4	1.0	45	6	55	10	47.86	161.8
5	1.0	65	4	80	20	51.24	159.2
6	0.5	45	6	55	20	52.14	144.8
7	0.5	65	4	55	20	56.44	123.5
8	1.5	45	4	55	30	51.43	164.8
9	0.5	45	2	55	20	55.99	107.8
10	1.0	65	2	55	20	55.83	124.4
11	1.0	65	6	55	20	51.88	164.3
12	1.0	65	4	30	20	56.99	120.3
13	1.0	45	4	55	20	52.22	128.7
14	1.0	45	4	80	10	47.57	143.6
15	0.5	45	4	55	30	55.77	123.8
16	1.5	45	2	55	20	52.52	137.4
17	1.0	45	6	55	30	51.72	174.8
18	1.5	45	4	30	20	54.35	129.2
19	1.0	25	4	55	30	55.13	124.8
20	1.0	25	6	55	20	51.53	133.8
21	1.0	45	2	80	20	50.85	143.2
22	1.0	45	4	30	30	55.29	124.8
23	1.5	45	6	55	20	48.66	174.6
24	0.5	25	4	55	20	56.28	98.8
25	0.5	45	4	30	20	56.31	108.4
26	1.0	45	4	55	20	52.12	129.5
27	1.5	45	4	80	20	47.64	183.5
28	1.5	65	4	55	20	53.13	163.2
29	1.0	45	4	80	30	50.14	173.8
30	0.5	45	4	55	10	51.75	117.6
31	1.0	45	2	55	30	53.92	143.7
32	1.0	45	4	30	10	52.71	103.7
33	1.0	25	4	30	20	56.31	94.2
34	1.0	45	6	30	20	52.38	133.8
35	1.0	25	2	55	20	55.38	103.6
36	1.0	45	2	55	10	52.07	99.8
37	1.0	25	4	55	10	52.71	104.8
38	1.0	45	6	80	20	47.03	184.4
39	1.0	65	4	55	30	55.61	151.3
40	1.5	25	4	55	20	52.78	128.6
41	0.5	45	4	80	20	52.49	143.8
42	1.5	45	4	55	10	49.37	148.6
Obtained data for testing precision of ANFIS models							
43	0.5	30	3	50	10	54.63	90.4
44	1.0	40	4	50	20	52.77	121.2
45	1.5	50	5	60	30	50.19	186.5
46	1.0	30	4	70	10	49.90	123.7
47	0.5	40	6	60	20	51.85	146.5
48	0.5	50	5	50	30	55.64	137.3
49	1.0	30	4	60	10	50.96	114.1
50	1.5	40	6	70	20	46.72	193.8
51	1.0	30	6	80	30	48.65	200.7

3 BURNISHING EXPERIMENT

The burnishing samples are made of the hardened steel AISI 4140 steel, which is intensively employed to produce piston rods and high-pressure bushings.

The pre-machined hole in the specimen is produced using the drilling and internal rough turning processes. The obtained dimensions are the length of 60.0 mm, the internal diameter of 28.0 mm, and the outer diameter of 42.0 mm, respectively. There are 51 specimens employed in all experiments. The average roughness and Vickers hardness of the pre-machined sample are 4.68 μm and 420.8 HV, respectively. The pre-machined tolerances of the internal hole are +/–0.05 mm.

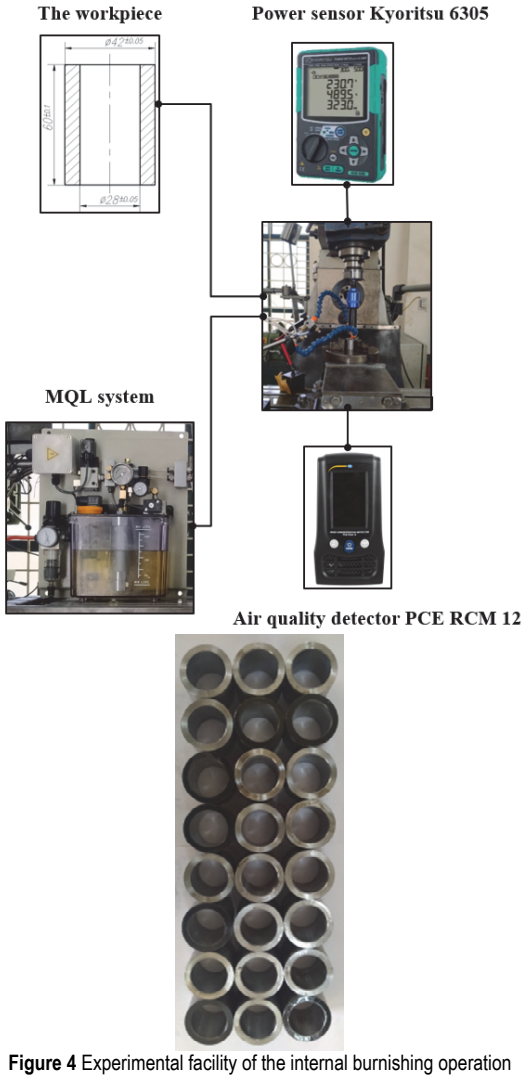

Figure 4 Experimental facility of the internal burnishing operation

The burnishing experiments are done with the aid of a vertical milling machine (Fig. 4). The tool having the assigned feed rate is moved along the *Z*-axis to obtain the desired length. The burnishing depth is adjusted using the micro-nut. The precision vise and jaw-centering chuck are used to clamp the workpiece. The MQL system is utilized to supply the oil mist into the burnishing region.

The power sensor and air quality detector are employed to capture the power and PM 2.5 values in the burnishing time. The experimental outcomes at the trial No. 14 are presented in Fig. 5.

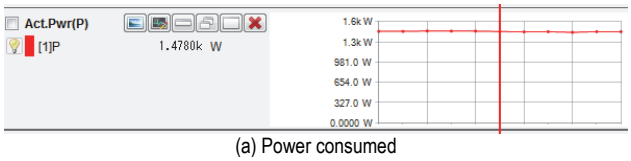

(a) Power consumed

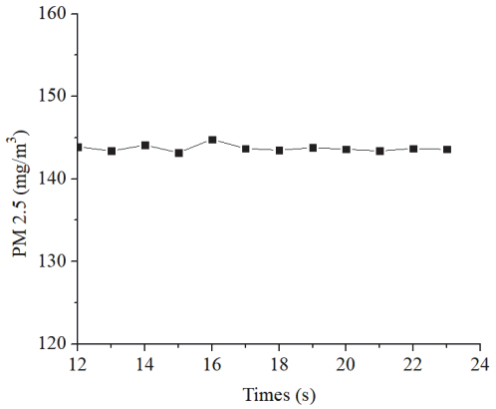

(b) Particle matter index

Figure 5 Representative results at the trial No. 14

4 RESULTS AND DISCUSSIONS

4.1 Development of the Optimal ANFIS Models

The experimental data are presented in Tab. 2. Four ANFIS parameters, including the number of input MFs (*N*), types of input MFs (*TI*), optimal method (*O*), types of output MFs (*TO*) are shown in Tab. 3. The computational training is conducted using the Taguchi matrix L_{16} to calculate the MSE values.

Table 3 The operating parameters for ANFIS models

Symbol	Level 1	Level 2	Level 3	Level 3
N	2	3	4	5
TI	trimf	trapmf	gaussmf	pimf
O	hybrid	backpropa		
TO	constant	linear		

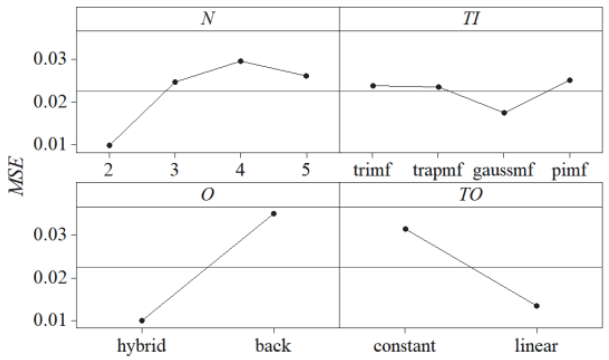

(a) For *EB* model

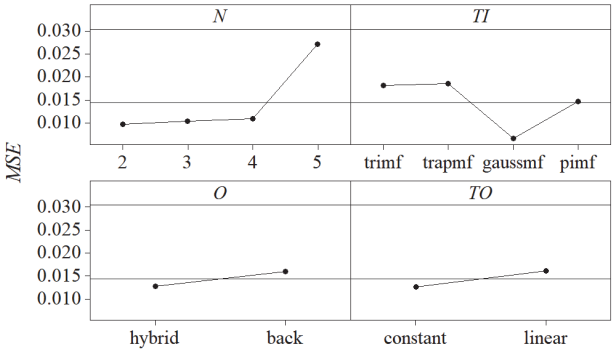

(b) For *PI* model

Figure 6 The effects of ANFIS parameters on the MSE values

As a result, for the *EB* model, the optimal data of the *N*, *TI*, *O*, and *TO* are 2, *gaussmf*, *hybrid*, and *linear*, respectively (Fig. 6a). For the *PI* model, the optimal data of the *N*, *TI*, *O*, and *TO* are 2, *gaussmf*, *hybrid*, and *constant*, respectively (Fig. 6b). Fig. 7 presents the ANFIS structure for performance measures. Fig. 8 illustrates the schematic rules for ANFIS models.

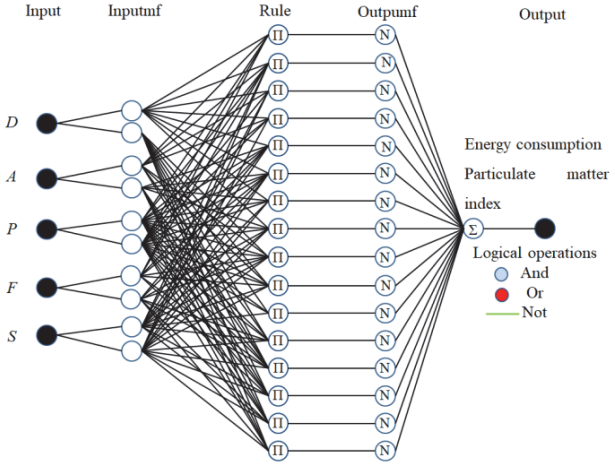

Figure 7 The ANFIS architecture for burnishing performances

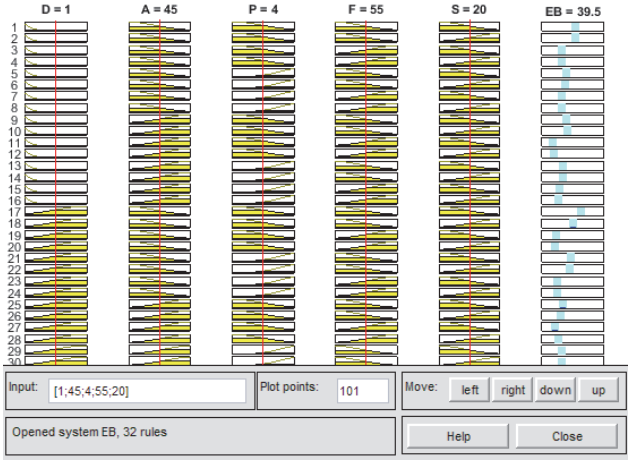

(a) For *EB* model

(b) For *PI* model

Figure 8 The schematic rules for ANFIS models

The comparisons between the experimental and predictive results are presented in Tab. 4. The errors of the *EB* and *PI* lie within the range of –1.12% to 1.25%, and -0.89% to 0.95%, respectively. The deviations indicate that the developed ANFIS models are accurate.

Table 4 Comparative errors for the burnishing responses

No.	*EB* / kJ			*PI* / mg/m^3		
	Exp.	ANFIS	Err. / %	Exp.	ANFIS	Err. / %
43	54.63	54.36	0.49	90.4	89.8	0.66
44	52.77	52.34	0.81	121.2	120.3	0.74
45	50.19	50.75	–1.12	186.5	186.9	–0.21
46	49.9	49.74	0.32	123.7	122.9	0.65
47	51.85	51.72	0.25	146.5	147.8	–0.89
48	55.64	55.54	0.18	137.3	137.9	–0.44
49	50.96	50.01	1.86	114.1	113.6	0.44
50	46.72	46.64	0.17	193.8	192.9	0.46
51	48.65	48.04	1.25	200.7	198.8	0.95
Exp.: Experimental value; Err.: Error						

4.2 ANOVA Results for Technological Responses

The ANOVA results of the *EB* and *PI* models are presented in Tabs. 5 and 6, respectively. The R^2 values of 0.9832 and 0.9863 indicate that the developed ANFIS correlations are adequate.

Table 5 ANOVA results for the *EB* model

So.	*SS*	*MS*	*F* value	*p*-value
Mo.	296.1024	14.8051	61.4575	< 0.0001
D	118.5507	118.5507	492.1157	< 0.0001
A	11.5362	11.5362	47.8878	0.0194
P	128.7738	128.7738	534.5529	< 0.0001
F	182.9845	182.9845	759.5868	< 0.0001
S	95.9473	95.9473	398.2867	< 0.0001
DF	50.3653	50.3653	209.0713	< 0.0001
DS	34.0458	34.0458	141.3275	0.0013
AF	11.1610	11.1610	46.3305	0.0039
PS	35.1713	35.1713	145.9995	0.0009
D^2	29.9190	29.9190	124.1969	0.0014
A^2	136.0894	136.0894	564.9208	< 0.0001
P^2	36.5781	36.5781	151.8395	0.0013
F^2	21.2904	21.2904	88.3784	0.0024
S^2	34.5148	34.5148	143.2742	0.0011
Residual	5.0595			
Cor Total	301.1619			
R^2 = 0.9832; Adjusted R^2 = 0.9764; Predicted R^2 = 0.9652				

Table 6 ANOVA results for *PI* model

So.	*SS*	*MS*	*F* value	*p*-value
Mo.	24260.3979	1213.0199	80.9812	< 0.0001
D	2096.5513	2096.5513	139.9660	< 0.0001
A	1697.7990	1697.7990	113.3453	< 0.0001
P	2433.2756	2433.2756	162.4458	< 0.0001
F	2769.9998	2769.9998	184.9255	< 0.0001
S	1364.6192	1364.6192	91.1022	< 0.0001
DA	319.0019	319.0019	21.2966	0.0065
DF	602.5591	602.5591	40.2269	0.0035
DS	320.7741	320.7741	21.4149	0.0064
AP	313.6852	313.6852	20.9417	0.0062
PS	990.6781	990.6781	66.1378	0.0023
FS	290.6462	290.6462	19.4036	0.0068
D^2	668.1317	668.1317	44.6046	0.0037
A^2	776.2379	776.2379	51.8217	0.0032
P^2	1128.9123	1128.9123	75.3663	0.0018
F^2	611.4203	611.4203	40.8185	0.0034
S^2	616.7370	616.7370	41.1734	0.0034
Residual	314.5595			
Cor Total	24574.9573			
R^2 = 0.9863; Adjusted R^2 = 0.9736; Predicted R^2 = 0.9642				

Single terms (*D*, *A*, *P*, *F*, and *S*), interactive terms (*DF*, *DS*, *AF*, and *PS*), and quadratic terms (D^2, A^2, P^2, F^2, and P^2) are significant factors. The *F* has the highest contribution of 19.51%, followed by the *P* (13.73%), *D* (12.64%), *S* (10.23%), and *A* (1.23%), respectively. The contributions of the *DF*, *DS*, *AF*, and *PS* are 5.37%, 3.36%, 1.19%, and 3.75%, respectively. The contributions of the D^2, A^2, P^2, F^2, and P^2 are 3.19%, 14.51%, 3.90%, 2.27%, and 3.68%, respectively.

Single terms (*D*, *A*, *P*, *F*, and *S*), interactive terms (*DF*, *DS*, *AF*, and *PS*), and quadratic terms (D^2, A^2, P^2, F^2, and P^2) are significant factors. The *F* has the highest contribution of 15.63%, followed by the *P* (13.73%), *D* (11.83%), *A* (9.58%), and *S* (7.70%), respectively. The contributions of the *DA*, *DF*, *DS*, *AP*, *PF*, and *PS* are 1.80%, 3.40%, 1.81%, 1.77%, 3.09%, and 5.59%, respectively. The contributions of the D^2, A^2, P^2, F^2, and P^2 are 3.77%, 4.38%, 6.37%, 3.45%, and 3.48%, respectively.

4.3 Influences of MQL Variables on the Responses

Fig. 9a presents that a higher *D* decreases the *EB* value. An increased nozzle diameter causes a higher droplet size, leading to a higher amount of fluid entering the machining region. The penetration of the oil mist is more effective, resulting in higher CL efficiency. The friction at the interfaces between the rollers and the surface to be machined decreases, leading to a reduction in the energy consumed. With the nozzle diameter of 0.5 mm, energy consumption is maximum, while the minimum energy is obtained at the nozzle diameter of 1.5 mm. A higher diameter causes a reduction in the machining forces that can be found in the turning [18] and milling [19] operations.

As shown in Fig. 9a, when the *A* changes from 25 to 45 deg., the *EB* value decreases. In contrast, when the *A* increases from 45 to 65 deg., the *EB* value increases. A higher inclined angle leads to a proper position of the nozzle and more lubricant enters the burnishing region. The CL efficiency enhances; hence, the energy consumption decreases. At the inclined angle of 45 deg., the oil mist toward the interface precisely, and the energy consumption is minimum. Further inclined angle (45 to 65 deg.) causes an improper position of the nozzle and the oil mist ineffectively enters into the interface; hence, the friction and resistance at the machining region increase. More energy is consumed to overcome the friction. At the inclined angle of 65 deg., energy consumption is maximum. Similar impacts of the inclined angle on the machining forces can be found in the works of [18, 19].

Fig. 9b presents that higher *P* decreases the *EB* value. The air pressure has an important role in decreasing the droplet size and increasing the velocity. When the *P* increases, the droplets with a smaller diameter have a better ability to penetrate into the burnishing zone, leading to higher CL efficiency. Higher fluid velocity increases the heat exchange in the burnishing area. Consequently, the friction at the interface decreases and the energy consumption reduces. A reduction in the energy consumption with higher air pressure is presented in the turning [19] and milling [20] operations.

Fig. 9b presents that a higher *F* decreases the *EB* value. An increased oil quantity increases the number of oil droplets entering the burnishing zone. The lubrication efficiency will be enhanced due to the frictional reduction. Moreover, the increase in oil quantity benefits an effective cooling at the interface. Therefore, low energy consumption is required at a higher *F*. A reduction in the

energy consumption with a higher oil quantity is presented in the turning [18] and milling [19] operations.

Fig. 9c presents the impact of the *S* on the *EB*. It can be stated that a higher *S* increases the *EB* value. The spraying distance has an important role in decreasing the droplet size and velocity of the oil mist. A shorter *S* causes a smaller droplet, leading to better penetration into the burnishing region. The CL efficiency increases; hence, the *EB* reduces. In contrast, an increased *S* decreases the amount of lubricant; hence, the friction increases and greater resistance is produced. Consequently, more energy is required to overcome the friction. A similar impact of the spraying distance on machining forces can be found in the work of [19].

Fig. 10a presents that a higher *D* increases the *PI* value. An increased diameter increases the oil quantity of lubricant in the oil mist, which is widely distributed into the air through MQL nozzles; hence, the *PI* value increases. A similar impact of the nozzle diameter on the particulate matter index can be found in the work of [16].

Fig. 10a presents that a higher *A* increases the *PI* value. When the inclined angle increases, a higher proportion of the oil mist evaporates into the surrounding environment, resulting in a higher value of the particulate matter index. A higher *PI* value with an increased inclined angle can be found in the work of [16].

Fig. 10b presents that a higher *P* causes an increase in the *PI* value. The reason is that air pressure has an important role in changing the droplet size and velocity of the oil mist. The droplets with a small diameter and higher velocity can easily distribute in the working space; hence, the value of the particulate matter index increases. A similar impact of the air pressure on the particulate matter index can be found in the work of [16].

Fig. 10b presents that an increased *F* causes a higher *PI* value. A higher oil quantity causes an increment in the amount of oil consumed and the number of oil droplets, which are easily distributed into the air; hence, the *PI* value increases. A higher *PI* value with an increased oil quantity is presented in the work of [16].

Fig. 10c presents that a higher *S* increases the *PI* value. When the spraying distance increases, a higher amount of the oil mist distributes into the air, resulting in a higher *PI*. A higher *PI* value with an increment in the spraying distance is presented in the work of [16].

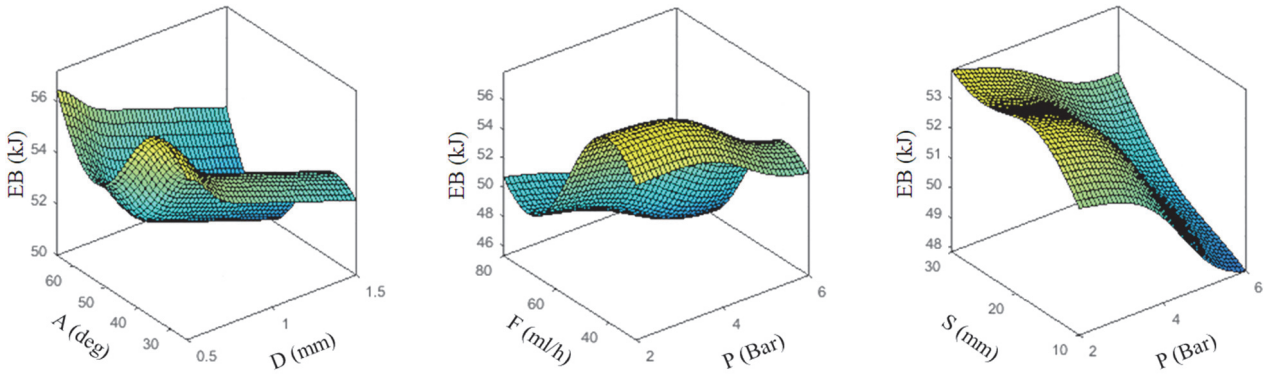

(a) *EB* versus *A* and *D* (b) *EB* versus *P* and *F* (c) *EB* versus *S* and *P*

Figure 9 The interactive influences of the MQL variables on the EB

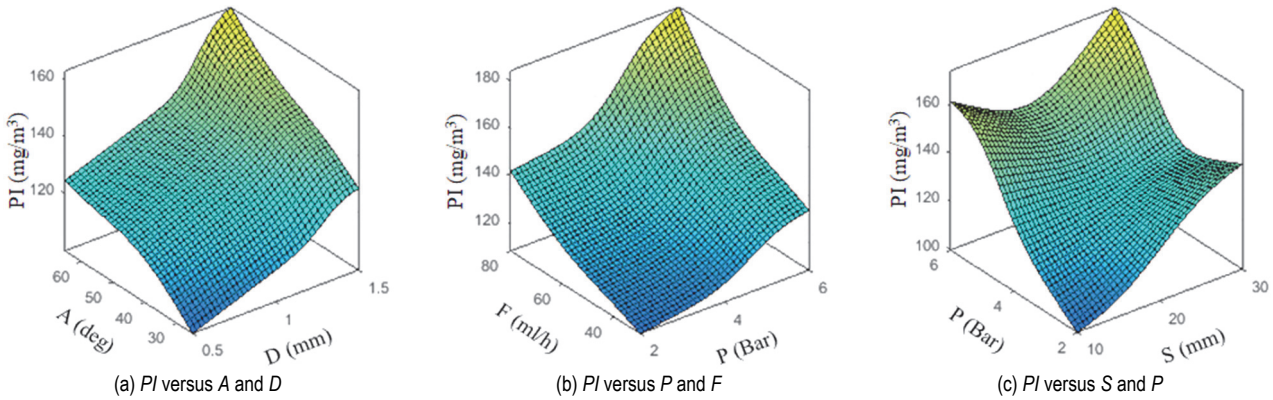

(a) *PI* versus *A* and *D* (b) *PI* versus *P* and *F* (c) *PI* versus *S* and *P*

Figure 10 The interactive influences of the *MQL* variables on the *PI*

4.4 Optimization Results

The optimal data are selected using the developed ANFIS models and the NSGA-G. The Pareto graph showing the relation between the *EB* and *PI* is presented in Fig. 11. As a result, the burnishing responses have a contradictory trend, in which a decreased *EB* relates to an increased *PI*. At the point 1, the minimum particulate matter index is obtained, while energy consumption is the highest. At the point 2, the lowest energy is observed, while the maximum particulate matter index is produced. Therefore, it is necessary to select a proper solution satisfying all requirements.

Three alternative solutions produced by the TOPSIS are presented in Tab. 7. As a result, the solution no. 131 is selected as the best solution. The optimum values of the *D*, *A*, *P*, *F*, and *S* are 1.0 mm, 35 deg., 3.0 Bar, 70 ml/h, and 10 mm, respectively. The reductions in the *EB* and *PI* are 8.0% and 15.7%, respectively (Tab. 8).

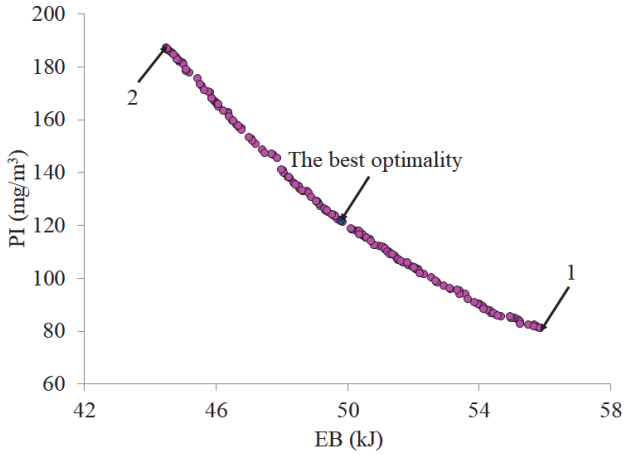

Figure 11 Pareto fronts produced by the NSGA-G

Table 7 Alternative solutions produced by the TOPSIS

No.	Optimization parameters					Responses		*SC*
	D	*A*	*P*	*F*	*S*	*EB*	*PI*	
131	1.0	35	3	70	10	49.62	121.2	0.762
264	1.0	33	3	77	10	49.73	123.7	0.751
378	0.9	32	3.5	75	10	50.12	120.2	0.748

Table 8 Optimization results generated by the NSGA-G

Method	Optimization parameters					Responses	
	D mm	*A* deg.	*P* Bar	*F* ml/h	*S* mm	*EB* kJ	*PI* mg/m³
Initial	1.0	45	2	55	30	53.92	143.7
Optimal	1.0	35	3	70	10	49.62	121.2
Redu. / %						8.0	15.7

It can be stated that optimal results are incorporated with parametric influences. The middle value of the *D* is applied to provide a sufficient amount of lubricant, resulting in reductions in the *EB* and *PI*. With the *A* of 35 deg., the oil mist mostly enters the interface; hence, reductions in the burnishing objectives are obtained. A decrease in the *P* causes higher droplet size and lower velocity, which results in a low *PI* value. An increment in the *F* causes higher CL efficiency and lower friction, leading to a reduction in the *EB*. A lower *A* increases the CL impact and decreases the distribution of the oil mist; hence, the *EB* and *PI* are simultaneously reduced.

The industrial remarks are expressed as:

The obtained data can be utilized to save the *EB* and *PI* values in the practical MQL-based burnishing process.

The optimal ANFIS correlations can be employed to accurately predict the outcomes of the *EB* and *PI* values in industrial applications.

The observed data can be utilized to develop the knowledge system related to burnishing processes.

The developed MQL system can be used as a significant recommendation to propose other CL devices.

5 CONCLUSIONS

In this study, the MQL variables were optimized to decrease the *EB* and *PI* of the internal burnishing process. The inputs were the *D*, *A*, *P*, *F*, and *S*. The performance measures were developed using optimal ANFIS models. The best solution was determined using the NSGA-G and TOPSIS. The conclusions are expressed as:

1. The maximum levels of the *D*, *P*, and *F* could be applied to reduce the *EB*, while the minimum *S* is recommended. Moreover, the middle level of the *A* could be utilized to save the *EB*. To decrease the *PI*, the minimum MQL variables were applied.

2. All MQL variables have effective contributions to the ANFIS correlations. For the *EB* model, the *F* had the highest contribution, followed by the *P*, *D*, *S*, and *A*, respectively. For the *PI* model, the *F* had the highest contribution, followed by the *P*, *D*, *A*, and *S*, respectively.

3. The ANFIS correlation having 2-2-2-2-2 structure could be used to develop the EB and PI models. The Taguchi method could be employed to select the optimal ANFIS models, instead of the arbitrary selection.

4. The optimal outcomes of the *D*, *A*, *P*, *F*, and *S* were 1.0 mm, 35 deg., 3 Bar, 70 ml/h, and 10 mm, respectively. The *EB* and *PI* were decreased by 8.0% and 15.7%, respectively, as compared to common values.

5. The impacts of the MQL variables on the wear rate, friction of coefficient, residual stress, and the total cost will be explored in further works.

6 REFERENCES

[1] Stalin John, M. R., Banerjee, N., Shrivastava, K., & Vinayagam, B. K. (2017). Optimization of roller burnishing process on EN-9 grade alloy steel using response surface methodology. *Journal of the Brazilian Society of Mechanical Sciences and Engineering*, *39*, 3089-3101. https://doi.org/10.1007/s40430-016-0674-8

[2] Nguyen, T. T. & Le, X. B. (2018). Optimization of interior roller burnishing process for improving surface quality. *Materials and Manufacturing Processes*, *33*(11), 1233-1241. https://doi.org/10.1080/10426914.2018.1453159

[3] Cagan, S. C., Buldum, B. B., & Ozkul, I. (2019). Experimental investigation on the ball burnishing of carbon fiber reinforced polymer. *Materials and Manufacturing Processes*, *34*(9), 1062-106. https://doi.org/10.1080/10426914.2019.1615078

[4] Prasad, K. A. & John, M. R. S. (2021). Optimization of external roller burnishing process on magnesium silicon carbide metal matrix composite using response surface methodology. *Journal of the Brazilian Society of Mechanical Sciences and Engineering*, *43*, 342. https://doi.org/10.1007/s40430-021-03069-3

[5] Nguyen, T. T. (2021). Multi-response performance optimization of burnishing operation for improving hole quality. *Journal of the Brazilian Society of Mechanical Sciences and Engineering*, *43*, 560. https://doi.org/10.1007/s40430-021-03274-0

[6] Van, A. L. & Nguyen, T. T. (2022). Investigation and optimization of mql system parameters in the roller-burnishing process of hardened steel. *Strojniski Vestnik - Journal of Mechanical Engineering*, *68*(3), 155-165. https://doi.org/10.5545/sv-jme.2021.7473

[7] Nguyen, T. T., Nguyen, T. A., Trinh, Q. H., Pham, L. H., & Le, X. B. (2022). Artificial neural network-based optimization of operating parameters for minimum quantity lubrication-assisted burnishing process in terms of surface characteristics. *Neural Computing and Applications*, *34*(9), 7005-7031. https://doi.org/10.1007/s00521-021-06834-6

[8] Sachin, B., Narendranath, S., & Chakradhar, D. (2019). Selection of optimal process parameters in sustainable diamond burnishing of 17-4 PH stainless steel. *Journal of the Brazilian Society of Mechanical Sciences and Engineering*, *41*, 219. https://doi.org/10.1007/s40430-019-1726-7

[9] Sachin, B., Narendranath, S., & Chakradhar, D. (2020). Application of desirability approach to optimize the control factors in cryogenic diamond burnishing. *Arabian Journal for Science and Engineering*, *45*, 1305-1317.

https://doi.org/10.1007/s13369-019-04326-3
[10] Revankar G. D., Shetty R., Rao, S. S., & Gaitonde, V. N. (2017). Wear resistance enhancement of titanium alloy (Ti-6Al-4V) by ball burnishing process. *Journal of Materials Research and Technology*, *6*(1), 13-32. https://doi.org/10.1016/j.jmrt.2016.03.007
[11] Attabi, S., Himour, A., Laouar, L., & Motallebzadeh, A. (2021). Effect of ball burnishing on surface roughness and wear of AISI 316L SS. *Journal of Bio- and Tribo-Corrosion*, *7*, 7. https://doi.org/10.1007/s40735-020-00437-9
[12] Nguyen, T. T., Cao, L. H., Dang, X. P., Nguyen, T. A., & Trinh, Q. H. (2019). Multi-objective optimization of the flat burnishing process for energy efficiency and surface characteristics. *Materials and Manufacturing Processes*, *34*(16), 1888-1901. https://doi.org/10.1080/10426914.2019.1689266
[13] Nguyen, T. T. & Le, M. T. (2021). Optimization of internal burnishing operation for energy efficiency, machined quality, and noise emission. *International Journal of Advanced Manufacturing Technology*, *114*, 2115-2139. https://doi.org/10.1007/s00170-021-06920-y
[14] Teimouri, R. & Amini, S. (2019). A comprehensive optimization of ultrasonic burnishing process regarding energy efficiency and workpiece quality. *Surface and Coatings Technology*, *375*, 229-242. https://doi.org/10.1016/j.surfcoat.2019.07.03
[15] Nguyen, T. T., Nguyen, T. A., Trinh, Q. H., & Le, X. B. (2022). Multi-Performance Optimization of Multi-Roller Burnishing Process in Sustainable Lubrication Condition. *Materials and Manufacturing Processes*, *37*(4), 407-427. https://doi.org/10.1080/10426914.2021.1962533
[16] Nguyen T. T. & Van, A. L. (2022). Machining and optimization of the external diamond burnishing operation. *Materials and Manufacturing Processes*. https://doi.org/10.1080/10426914.2022.2072880
[17] Vellingiri, E., Kalimuthu, V. K., & Samydurai, G. (2021). Fuzzy logic based dsr trust estimation routing protocol for MANET using evolutionary algorithms. *Tehnički vjesnik*, *28*(6), 2006-2014. https://doi.org/10.17559/TV-20200612102818
[18] Zaman, P. B. & Dhar, N. R. (2020). Multi-objective optimization of double-jet mql system parameters meant for enhancing the turning performance of Ti-6Al-4V Alloy. *Arabian Journal for Science and Engineering*, *45*, 9505-9526. https://doi.org/10.1007/s13369-020-04806-x
[19] Liu, Z. Q., Cai, X. J., Chen, M., & An, Q. L. (2011). Investigation of cutting force and temperature of end-milling Ti-6Al-4V with different minimum quantity lubrication (MQL) parameters. *Journal of Engineering Manufacture*, *225*(8), 1273-1279. https://doi.org/10.1177/2041297510393793

Contact information:

An-Le VAN
Faculty of Engineering and Technology, Nguyen Tat Thanh University,
300A Nguyen Tat Thanh Street, Ward 13, District 4,
Ho Chi Minh City 70000, Vietnam
E-mail: lvan@ntt.edu.vn

Trung-Thanh NGUYEN
(Corresponding author)
Faculty of Mechanical Engineering, Le Quy Don Technical University,
236 Hoang Quoc Viet, Ha Noi 100000, Vietnam
E-mail: trungthanhnguyen@lqdtu.edu.vn